

PPP Integrity for Advanced Applications, Including Field Trials with Galileo, Geodetic and Low-Cost Receivers and a Preliminary Safety Analysis

Navarro Madrid, P. F., Martínez Fernández, L., Alonso López, M., Laínez Samper, M. D., Romay Merino, M. M., *GMV*

BIOGRAPHIES

Pedro F. Navarro Madrid holds a Master of Science in Mathematics from the University of Murcia (Spain) and Postgraduate studies in Theoretical Physics at the University of Valencia (Spain). He has worked at GMV since 2002 as an engineer in the development of Galileo and later in R&D activities covering both the ground and user segments.

Laura Martínez Fernández holds a Degree in Aerospace Engineering from Polytechnic University of Valencia, specialty in Aero-navigation, and an MSc in Aeronautical Engineering from Polytechnic University of Catalonia, specialty in Space. When Laura Martínez finished her internship in GMV, she joined GMV as GNSS engineer at the GMV GNSS Business Unit, participating in activities related with magicGNSS, a suite of tools for GNSS data processing featuring high precision and integrity.

María Alonso López has a licentiate degree in Mathematics from the University of Alicante and a Master's degree in Mathematical Engineering from the Madrid Complutense University. She works in GMV as safety & dependability engineer and has been responsible for RAMS in several projects in the Galileo programme, as well as in the design and production of the A400M Cargo Crane System.

María D. Laínez Samper is currently coordinating the GMV research activities in the field of Satellite Navigation, and in particular those related to precise positioning applications. She has also worked in experimentation and verification activities, in the Operational Systems Division, during the preliminary phases of the Galileo Program, and has been the responsible for the clock prediction and navigation message computation modules in the Galileo E-OSPF (Experimental Orbitography and Synchronization Processing Facility).

Miguel M. Romay Merino is the GNSS Business Unit Director at GMV Aerospace and Defence. Miguel leads the GMV Unit that has become one of the strongest groups of GNSS experts thanks to its key involvement in GPS,

EGNOS and Galileo. Miguel has been a pioneer in the Galileo Program, collaborating on aspects such as constellation design, precise orbit determination, integrity, performance evaluation, system definition, etc. Miguel is today involved in GMV research activities in the definition of novel GNSS applications and on the design of new generation GNSS.

ABSTRACT

Precise Point Positioning (PPP) is a consolidated high precision positioning technique providing centimetre-level error. PPP processes dual-frequency pseudorange and carrier-phase measurements from a single user receiver, using detailed physical models and precise GNSS orbit & clock products calculated beforehand, but it can also work with single-frequency receivers, significantly enhancing the receiver PVT solutions, in either the double and in the single frequency cases. PPP provides absolute positioning as opposed to relative techniques such as RTK (Real Time Kinematics). PPP can be applied to both post-processing and real-time applications, provided that real-time input orbit and clock data are available.

In the last years, we have been working in developing an integrity layer to be added to the PPP positioning solution, necessary for the provision of certain critical applications. One of the main features of this integrity approach is that it combines in a well-balanced way, information from the system and information from the user, in order to build optimum horizontal and vertical protection levels. Besides this, and tightly related to the final application, additional sources of information for complementing the integrity information can be considered, such as consistency checks with non-GNSS measurements, for example.

Previous work showed the excellent bounding capabilities of the KIPL algorithm for PPP integrity/reliability computation, considering three different scenarios: static, kinematic and convergence. Analyses have been extended based on the new *magicPPP* capability to simulate real time processing in post-processing mode. Additional tests have been carried out, including:

- Extend static testing, covering a several months long time period

- Double Frequency (DF, geodetic) and Single Frequency (SF, low cost) kinematic PPP testing, for covering a wide range of markets and applications.
- Dedicated experimentation for analysing different convergence periods, both in the double and single frequency contexts
- Multi-constellation testing, including Galileo

PPP integrity/reliability performances will be provided for the different testing conditions, in terms of protection level magnitude, and percentage of integrity failures for different integrity risk levels.

The field trials will be complemented with a preliminary safety analysis, aimed at:

- Detecting potential weaknesses in the current PPP integrity algorithm approach, to be overcome with future enhancements of the KIPL design and/or implementation.
- Being the first step towards a potential certification process, which could grant the use of the PPP integrity bounds for a wide range of high precision services and applications.

INTRODUCTION

Apart from the obvious need of integrity for safety critical applications, including aviation, road, LBS (emergency caller location), rail and maritime, recent market analyses, see [Ref. 3.], have drawn attention about the benefit of improved robustness and integrity for liability critical applications such as road (tolling operators, insurance telematics), LBS (mobile payments), maritime (fisheries, marine park management). While high-accuracy techniques as PPP or RTK are more and more widely used, and being these techniques every day closer to be compatible with mass-market GNSS devices, the advantages of an integrity layer for this type of applications is becoming palpable.

This paper will start with a brief introduction to our integrity concept for PPP solutions and a summary of its evolution from an empirical bound construction, based on a series of relevant indicators, to the current robust implementation. With a sound statistical foundation behind, it is able to compute real time horizontal and vertical protection levels for PPP positioning errors, given any user-defined confidence level.

With that scope, a series of relevant field trials have been carried out for demonstrating the PPP integrity algorithm bounding capabilities. The results will be presented next, showing Stanford diagrams and accuracy versus integrity analyses. Exhaustive tests in both static and kinematic modes have been carried out, in open sky and in more demanding environments, with geodetic receivers as well as with low-cost single frequency equipment. The test results show centimetric to decimetric protection levels for open-sky environments with geodetic receivers, and decimetric to sub-metric protection levels for more

degraded environments (urban and sub-urban) and/or with low-cost receivers. In addition, the outputs of a preliminary safety analysis have been summarised in a dedicated section, leading to relevant conclusions and interesting recommendations to be incorporated as ideas for improvement for the KIPL PPP integrity algorithm. This preliminary safety analysis includes a high level failure mode and effects analysis and a basic fault tree analysis.

All the PPP and PPP integrity processes have been carried out using the *magicGNSS* suite of products, including the *magicPPP* service (see [Ref. 28.]) for the generation of orbit and clock products, and the *magicPPP* client, now compatible with Android-based devices. We have developed the algorithms and the data processing infrastructure needed for providing a real-time PPP service. All the required components, from the real time orbit and clock products generation, to the PPP filter implementation and the service management, are under our responsibility, including obviously the PPP integrity bounds generation. All the *magicGNSS* suite products have been evolved for the current multi-constellation environment, and are able to support multi-processing with GPS, Glonass, Galileo, Beidou and QZSS. It is remarkable how the processing of Galileo satellites on top of GPS and Glonass leads to significant improvement in the PPP solution in terms of positioning accuracy see [Ref. 9.] and [Ref. 15.]. For this reason, and taking into account that eleven Galileo satellites are already available, and two more under commissioning phase at the moment of writing this paper, we will show the particular integrity results including the processing of Galileo. It is important to remark the new *magicPPP* capability for simulating real time processing in post-processing mode. Both measurements and products, as available for the real-time processing, can be archived for being used later on in subsequent real-time like post-processing. The PPP performances are slightly inferior than those obtained when using post-processed products, which are slightly more accurate, but it is clear that these real-time based outputs are certainly more realistic and much more representative of what can be expected to be obtained in real PPP applications, including the associated integrity bounds.

In summary, we are presenting the latest updates on our well-balanced, rigorously formulated integrity concept for PPP. We are assessing its feasibility in a series of field trials, covering a wide range of environments and user conditions, and finally we are complementing it with a preliminary safety analysis. With this, we want to show that there is a viable solution for advanced precise positioning applications requiring an additional integrity layer, or which would interestingly be enhanced with it as a complementary feature, such as agriculture, transport, construction, etc.

THE PPP TECHNIQUE AND *magicPPP*

PPP is a position location process which performs precise position determination using undifferenced dual-frequency



Figure 2: *magicAPK*, *magicPPP* client

All the *magicGNSS* suite products have been evolved for the current multi-constellation environment, and are able to support multi-processing with GPS, Glonass, Galileo, Beidou and QZSS. See [Ref. 4.] and [Ref. 5.] for further information about *magicGNSS*.

GMV Contribution to IGS

Back in 2010, GMV started participating as Analysis Centre for the Real Time IGS Pilot Project (<http://www.rtigs.net/index.php>), by processing data from a worldwide network of stations and providing precise predictions of GPS and GLONASS orbits and clocks, which are calculated using *magicGNSS*. Its contribution is still ongoing once Real Time IGS Project became operational in 2012.

Standard 2-day-long ODTs processes are executed every 15 minutes in order to generate real time orbit predictions, whereas real time clock data are generated at 1 second execution rate, via an auxiliary RT_CLK process. The mentioned process estimates the satellite clocks in real time taking as input the pre-processed observations coming from PPV and the outputs from the last ODTs execution. The real-time orbits and clocks generated this way can be used for feeding *magicGNSS* RT PPP processes, and can be stored in standard formats (SP3, clock RINEX) for post-processing analyses.

The *magicGNSS* products generation includes the execution of an offline ODTs process which runs in off-line post-processing mode with a latency of 2 days and specific setup. It generates orbit and clock products more accurate than the real time ones. When available, they can be used for feeding off-line PPP processes.

The comparison of real-time (RT) and off-line products, orbits and clocks, with respect to IGS, is shown in Figure 3 (orbits) and Figure 4 (clocks) below. Real time typical orbit accuracy is about 5-6 cm (4 cm after the last server upgrade), RMS, and typical real time clock sigma is about 3-4 cm. Analogous accuracies for the off-line products are around 2.5 cm for the orbits RMS, and around 2 cm for the clock sigma.

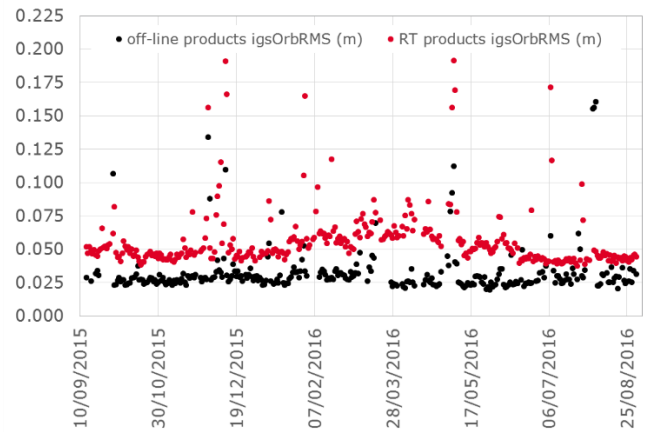


Figure 3: GPS Orbit comparison between IGS products and *magicGNSS* products (off-line and RT)

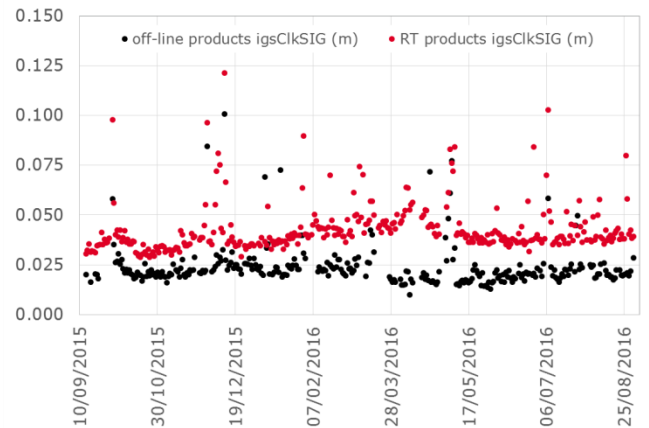


Figure 4: GPS Clock comparison between IGS products and *magicGNSS* products (off-line and RT)

For GLONASS, the comparison with respect to ESOC (European Space Operations Centre) products, since IGS does not provide analogue reference products for GLONASS, is slight higher than for GPS. For example, it stays around 10 cm for the orbits RMS.

magicGNSS does also process Galileo data. Precise orbit and clock products can be computed, and fed into PPP processes. The first PPP results obtained with *magicPPP* with Galileo are reported in [Ref. 11.]. See [Ref. 8.] and [Ref. 11.] for further information about the *magicPPP* off-line and real time services, and [Ref. 15.] for the latest results about multi-GNSS PPP performances including Galileo.

PPP Processing Modes

The PPP algorithm has traditionally used the iono-free combination of measurements at two different frequencies to cancel the ionospheric delay. This is a reasonable approach, since the ionospheric delay is not easy to model and estimate, in contrast with the case of the tropospheric delay. However, the iono-free combination has almost three times the noise of a single-frequency measurement. Thus, the option of using measurements of different

frequencies in the PPP, while correcting and/or estimating the ionospheric delay, should be also considered. In fact, the results presented in the following sections show that this second processing mode improves the reconvergence of the PPP algorithm after the carrier-phase tracking is reset for several satellites (e.g. when passing under a bridge). This convergence can be improved by using the fact that the jump in the ambiguity after the gap must equal an integer number times the wavelength of the signal (“gap bridging”).

magicPPP is able to run in the three following processing modes, regarding the different allowed measurements combinations:

- Iono-free, processing two different frequencies, and performing the corresponding iono-free combination
- Single Frequency, processing measurements from a single frequency channel
- Double Frequency, processing two different frequencies and performing both the iono-free and the geometry-free combinations

The gap-bridging option can be activated in both in the Single Frequency and Double Frequency modes.

The results presented in the current work have been obtained by processing different scenarios in either the Double Frequency or in the Single Frequency modes, depending on the receiver category: geodetic (Double Frequency) or low-cost (Single Frequency).

PPP INTEGRITY COMPUTATION

Experimental PPP Bounding Algorithm

The observed robustness of the PPP processes and the high accuracy of the obtained solutions motivated us to investigate on integrity algorithms for PPP. We have been working since 2012 in order to lay down a general integrity concept for the PPP solutions, following a practical service oriented approximation. With this we mean that we were not restricted to either pure system integrity or to integrity at user level only. Instead, we were looking for the most favourable combination of significant indicators we could assess. We started performing accuracy versus integrity analyses, trying to detect and study the different failure modes of the PPP processes. We analysed the PPP processes in detail, understanding that essential limitations for the attainable performances were linked to geometrical effects of the GNSS constellation, the quality of the orbit and clock products used as inputs, and the real-time reference systems realization. Relevant indicators were identified, and a preliminary integrity/reliability algorithm was designed.



Figure 5: Preliminarily identified PPP integrity/reliability indicators

Then the system was empirically tuned and evaluated in several field scenarios emulating real time operations, including static and kinematic use cases, different visibility conditions (open sky and occultation with different types of obstacles such as trees or buildings), and communication losses of different durations. Figure 6 below shows the preliminary PPP integrity/reliability algorithm performances, vertical protection level (PL) versus vertical error, in a kinematic scenario:

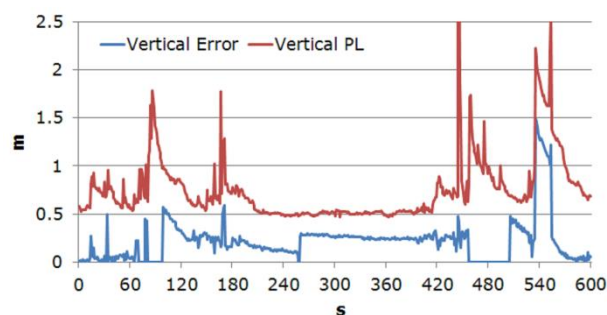


Figure 6: Preliminary PPP integrity/reliability algorithm performances: vertical PL vs error

We got to conclude that it should be feasible to define a specific algorithm able to bound the PPP errors, taking into account the identified relevant indicators, providing vertical and horizontal protection levels in the range of a few decimetres, with a low percentage of integrity failures. The weakness of the preliminary algorithm, though it worked quite well, was that it lacked a rigorous mathematical formulation. It followed an ‘ad hoc’ expression which had been empirically tuned for fitting all the analysed scenarios. The challenge was there: finding a comprehensive approach, statistically sound and mathematically rigorous, able to replace the observational preliminary computation. Further details can be consulted in the following references: [Ref. 10.],[Ref. 11.] and [Ref. 12.].

General Integrity Method for a Kalman Filter Navigation Solution and PPP Bounding Computation

The task of building an integrity algorithm as described above, based on solid foundations, requires solving two main problems:

- Statistically characterize the different error sources: measurements, PPP products, etc. If possible, in real-time: for instance, measurement errors should be characterized by using the PPP residuals indicators.
- Compute a statistical distribution of the solution error that combines the different error sources according to the Kalman equations.

In fact, the general solution to these problems applies for any Kalman navigation solution. The particularities of the PPP algorithm will be later taken into account to tailor this general method.

The starting point to define such a method was the IBPL technique (Isotropy-Based Protection Level), an integrity method for PVT least-squares solutions, that has successfully addressed the associated difficulties (see references [Ref. 16.], [Ref. 17.], [Ref. 18.], [Ref. 19.] and associated patent [Ref. 1.]). The IBPL method assumes basically no a priori knowledge on either the size or the pointing direction of the vector of measurement errors, which leads to the so-called isotropy assumption that all possible pointing directions are equally probable. IBPL has proven highly reliable in all kinds of environments thanks to the simplicity of its assumptions. Although IBPL only applies to a least-squares solution, its ground idea and its mathematical development are very useful in the general approach to the filtered case.

One of the main motivations to develop the IBPL algorithm was the insufficiency of the classical integrity concepts developed for the aviation domain, such as GBAS/SBAS or RAIM, to provide a reliable integrity concept for land users. Land users, and very especially urban users, are exposed to local sources of errors that very often become the primary contributors to the total error budget. These local effects include multipath, Non-Line-Of-Sight tracking (NLOS), and carrier-phase ambiguities discontinuities due to obstacles such as trees or buildings, which depend on the immediate vicinity of the user. Errors of this type are very frequent (hence they often take place simultaneously) and extremely difficult to model in a statistical sense as they are highly dependent on the peculiarities of the local environment. An integrity algorithm is needed that first of all covers these changing degraded conditions, which are indeed quite frequent. In particular, it must be autonomous and not relying in restrictive statistical assumptions on the measurement errors.

The IBPL method is based in the concept of Protection Level, as the new method developed for Kalman filters. A (horizontal or vertical) protection level is a number that bounds the (horizontal or vertical) position error, so that

the probability of this error exceeding the protection level is smaller than or equal to the integrity risk α . More demanding integrity requirements thus imply a smaller value of α . When the protection level exceeds a certain threshold, usually called alarm limit, the system is declared unavailable. There is always a tension between the requirements of integrity and availability.

In the case of a solution from a Kalman-filter the new technique has to address several additional challenges:

- The integrity bounds should reflect the improved filter performance, being much smaller than those computed for the least-squares.
- The filter makes use of different types of measurements: pseudoranges, carrier-phase, with different characteristics of noise.
- The filter solution combines observations from different epochs, in a possibly changing environment.
- The temporal correlation of measurements, with a great impact in the performance of the filtered solution, must be accounted for.

The first point is important, since for many applications, such as automatic driving, the size of the Protection Levels must be relatively small, or else the system will be permanently unavailable.

A generalization of the IBPL method valid for the Kalman processing case, was developed, and applied to the computation of the bounds (Protection Levels) to the PPP solution problem. It incorporated all the experience gathered in the previous experimental phase, and added a rigorous mathematical layer on top of it. It was introduced as KIPL (Kalman Integrated Protection Level), and was tested with excellent results, both for low-cost as well as for geodetic receivers, in different testing environments, see [Ref. 13.], [Ref. 14.] and [Ref. 22.]. As IBPL, KIPL is basically an autonomous method, although it can also process external information about the quality of the satellite orbit and clock products.

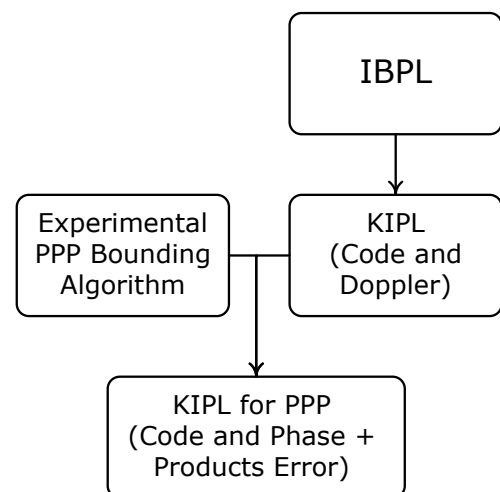


Figure 7: PPP integrity method development outline

The KIPL algorithm has been implemented in our PPP client, *magicPPP*. All the results presented in this paper have been obtained using *magicPPP* to compute the navigation solution and the associated Protection Levels.

SIX EXAMPLE TEST CASES

This section is aimed at extending the first and promising results obtained with the KIPL reported in [Ref. 13.], [Ref. 14.]. The new tests illustrate the behaviour of the KIPL algorithm in slightly more challenging conditions, including:

- Extensive analysis in static scenario, compiling a large data set (four months) and allowing different integrity/reliability analyses such as Stanford diagrams, and safety index vs number of integrity failures charts.
- Analyses in kinematic scenarios, including Galileo satellites in the process. The Galileo signal E5 is robust in circumstances where the GPS L2P signal can be lost, see [Ref. 9.].
- Analyses with more challenging single frequency low-cost receivers, for road and urban environments applications.
- Further research for smaller target integrity risks.
- Use of real-time orbit and clock products, which, as mentioned in the introductory sections, leads to realistic and highly representative results for real PPP applications.

Again, dedicated tests have been carried out for assessing the KIPL performances in static PPP, PPP in convergence period and kinematic PPP. In each one of the considered cases, the percentage of integrity failures for different target integrity risks is provided, together with integrity versus accuracy plots, showing the PPP horizontal and vertical errors and the associated KIPL protection levels for certain given integrity risk values.

These examples are aimed at illustrating the huge potential of the KIPL bounding algorithm in different environmental circumstances. Note that in all the considered cases, the KIPL configuration is the same, except for the receiver kind associated parameters, and that it is the algorithm itself that is capable of fitting all the considered circumstances: static, kinematic, convergence, multi-constellation, gap-bridging, etc. In summary, it will be shown that the algorithm provides relatively small protection levels, automatically adapted to the conditions and complying with the integrity requirements.

As mentioned previously, the results have been obtained by using *magicPPP* as PPP client, and *magicGNSS* to provide real-time satellite orbit and clock corrections.

Test Case 1: Extensive Static: GPS + GLONASS

This test is based on the processing of four months (may-august 2017) of data from the GAP4 station (geodetic receiver, Topcon NetG5) located in the

GMV premises (see Figure 8 and Figure 9). The configuration of the PPP process is the same as in the convergence and kinematic Test Cases carried out with a geodetic receiver, i.e. Test Case 2, Test Case 4 and Test Case 3, this means that the process does not assume that the receiver is at rest for this static Test Case. Figure 8 below shows the GAP4 stations receiver and antenna location. The data processed includes GPS and GLONASS satellites.



Figure 8: GAP4 Station: receiver (left) and antenna (right)



Figure 9: GAP4 Station Location

Table 1 below contains the experimental rate of integrity failures for six different integrity risk values, for horizontal and vertical errors. The table columns contain the experimental rate of integrity failures, compared to the target integrity risk (TIR). This metric is computed by taking, for each target integrity risk, the overall fraction of epochs where the error is above the Protection Level and normalizing by the corresponding TIR. Hence, the integrity algorithm complies with the TIR whenever the metric is equal to or below 1. Although the bigger values of TIR do not correspond to realistic integrity requirements, they appear here to show the capability of the integrity algorithm to provide valid bounds for a wide range of values, based on an appropriate estimation of the solution error distribution.

Table 1: Relative (normalised with respect to Integrity Risk) rate of integrity failures in static scenario for different Target Integrity Risks (TIR) values

TIR	0.1	0.05	0.01	0.001	1e-04	1e-07
H	0.49	0.41	0.22	0.25	0.1	0
V	0.56	0.44	0.16	0	0	0

For better illustrating the obtained results, some plots have been generated, some of them showing the obtained Protection Levels (PLs) covering the horizontal and vertical errors as a function of time, for different TIR values, and one example of Stanford diagram for an TIR as demanding as 1e-07:

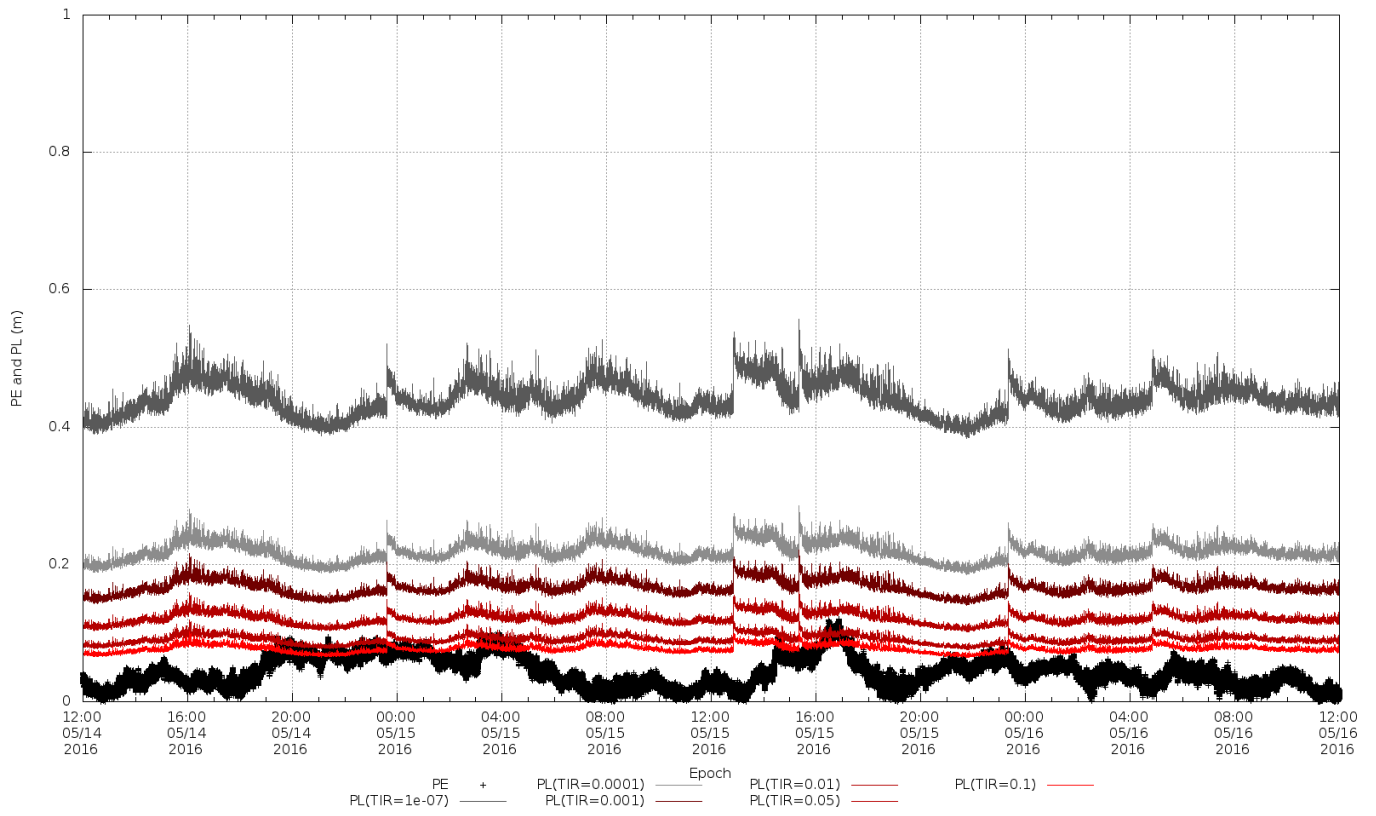


Figure 10: Position Error and PL - Horizontal

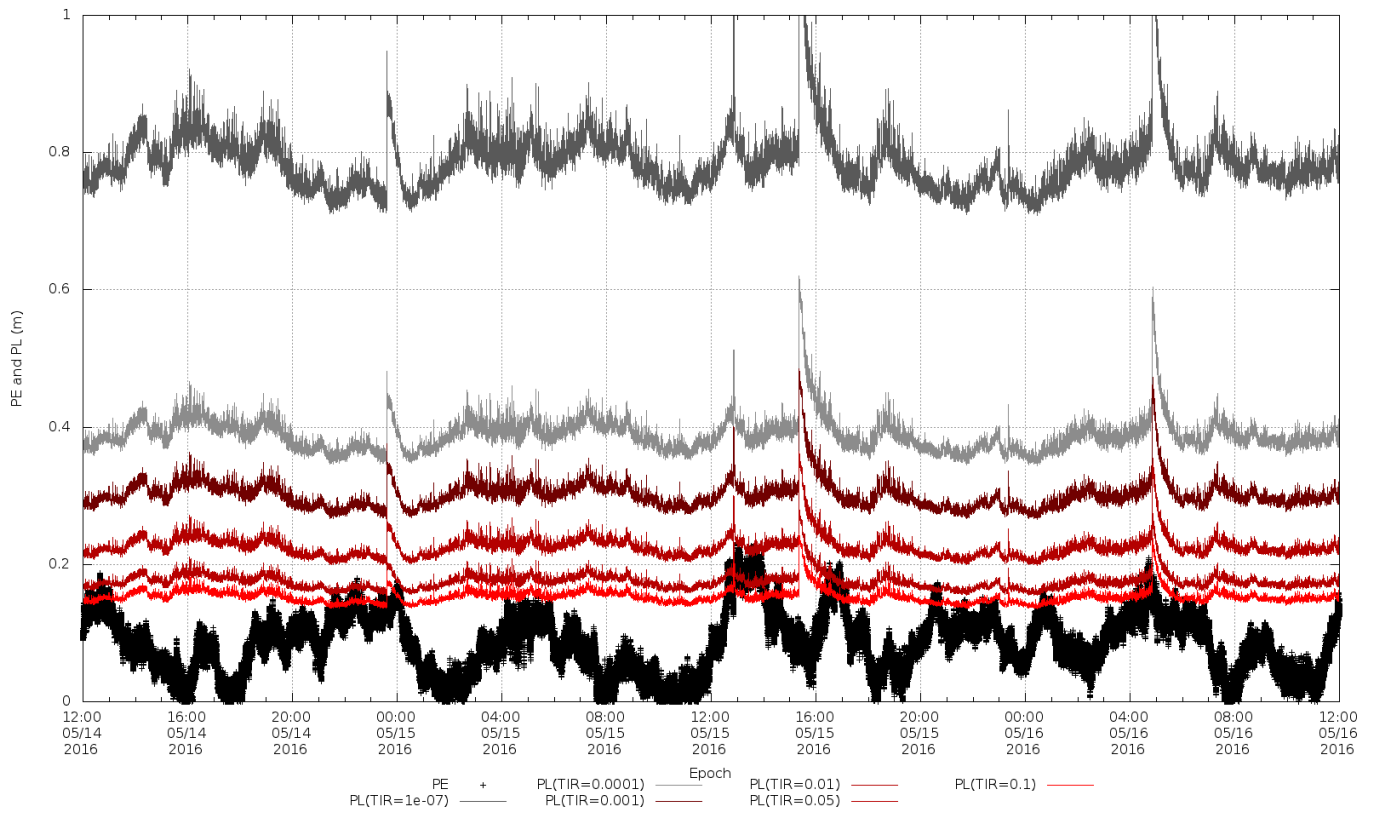


Figure 11: Position Error and PL - Vertical

Figure 12 below shows the horizontal error versus horizontal PL, for IR=1e-07. It can be observed that the PLs are typically between 0.4 and 1 m.

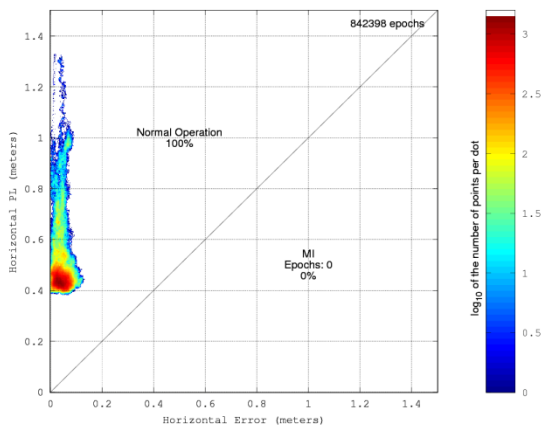


Figure 12: Stanford Diagram – Horizontal, TIR=1e-07

As we can see, the integrity algorithm provides protection levels values of a few decimetres in this type of scenario, which are representative of open-sky conditions.

Test Case 2: Convergence 1: Geodetic receiver

An important feature of the PPP navigation solutions is that the nominal accuracy is only reached after a certain period of time ('convergence time') that can range from a few

minutes to more than half an hour, depending on the characteristics of the scenario. The integrity bounds should evolve accordingly, decreasing at a similar rate as the solution error. The results of current section show how the considered integrity algorithm is capable of automatically reproducing the PPP solution behaviour even during the convergence periods. Note that the use of local corrections is able to largely mitigate the convergence difficulties, reducing it to just a few minutes, both in the double and frequency cases. We are internally working on a solution for solving the convergence problem, and will soon be able to provide bounding for the PPP solutions in assisted fast convergences.

The test was carried out forcing the PPP algorithm to reconverge every two hours, for twelve times, covering a total testing period of 24 hours.

Table 2 contains the experimental rate of integrity failures for the six considered integrity risk values, for horizontal and vertical errors, which is within target in all cases. The interpretation is the same as in Table 1.

Table 2: Relative rate of integrity failures in Test Case 2 for different Target Integrity Risks (TIR) values

TIR	0.1	0.05	0.01	0.001	1e-04	1e-07
H	0.83	0.63	0.39	0.17	0	0
V	0.44	0.19	0.07	0	0	0

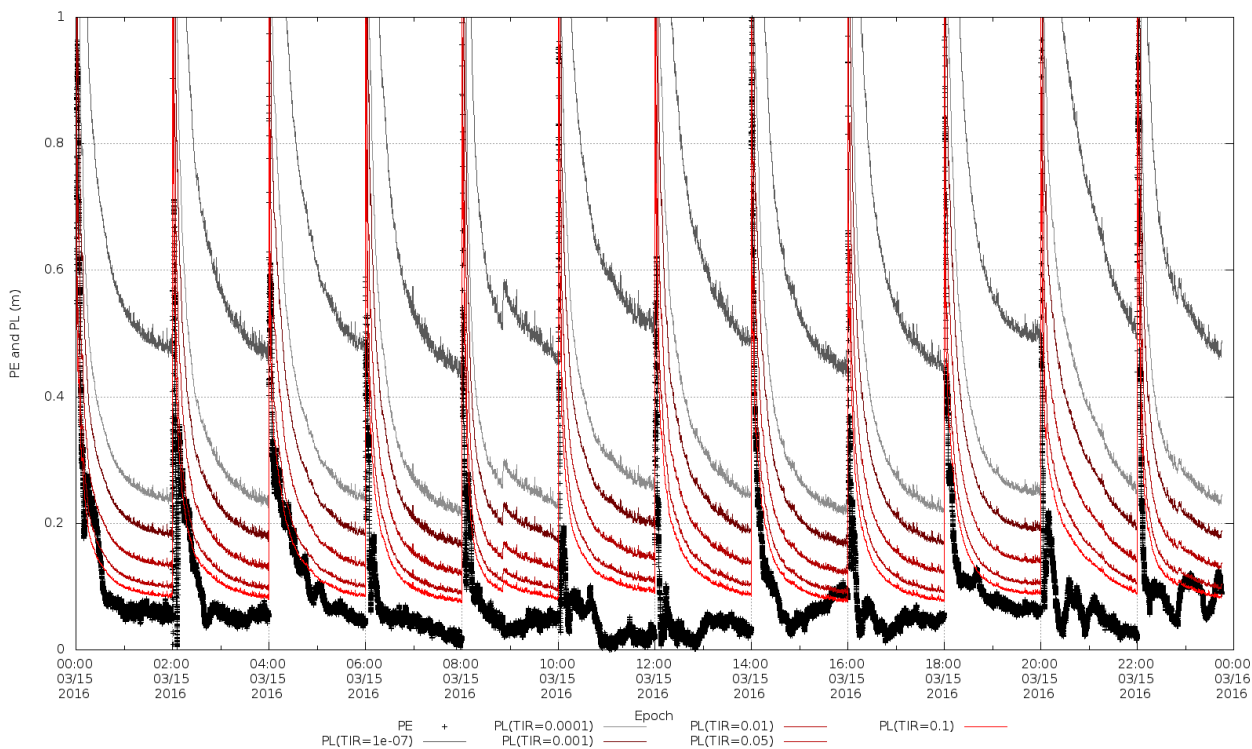


Figure 13: Position Error and PL - Horizontal

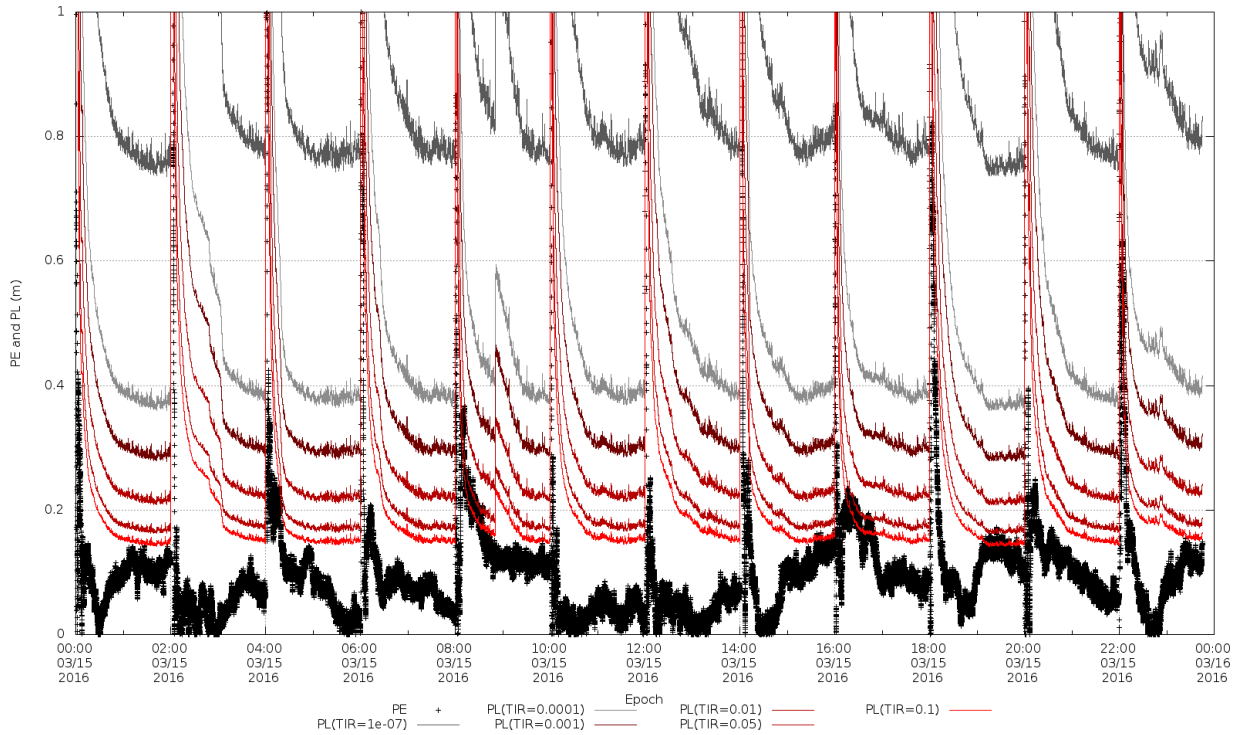


Figure 14: Position Error and PL - Vertical

Test Case 3: Convergence 2: Low-cost receiver.

As in the previous Test Case, the test was carried out forcing the PPP algorithm to reconverge every two hours, for twelve times, covering a total testing period of 24 hours. Table 3 Table 4 contains the experimental rate of integrity failures for the six considered integrity risk values, for horizontal and vertical errors, which is below the target in all cases.

Table 3: Relative rate of integrity failures in Test Case 3 for different Target Integrity Risk (TIR) values

TIR	0.1	0.05	0.01	0.001	1e-04	1e-07
H	0.47	0.55	0.42	0	0	0
V	0.68	0.90	0.65	0	0	0

Figures below are presented in order to show the behaviour of the Protection Levels for both horizontal and vertical case.

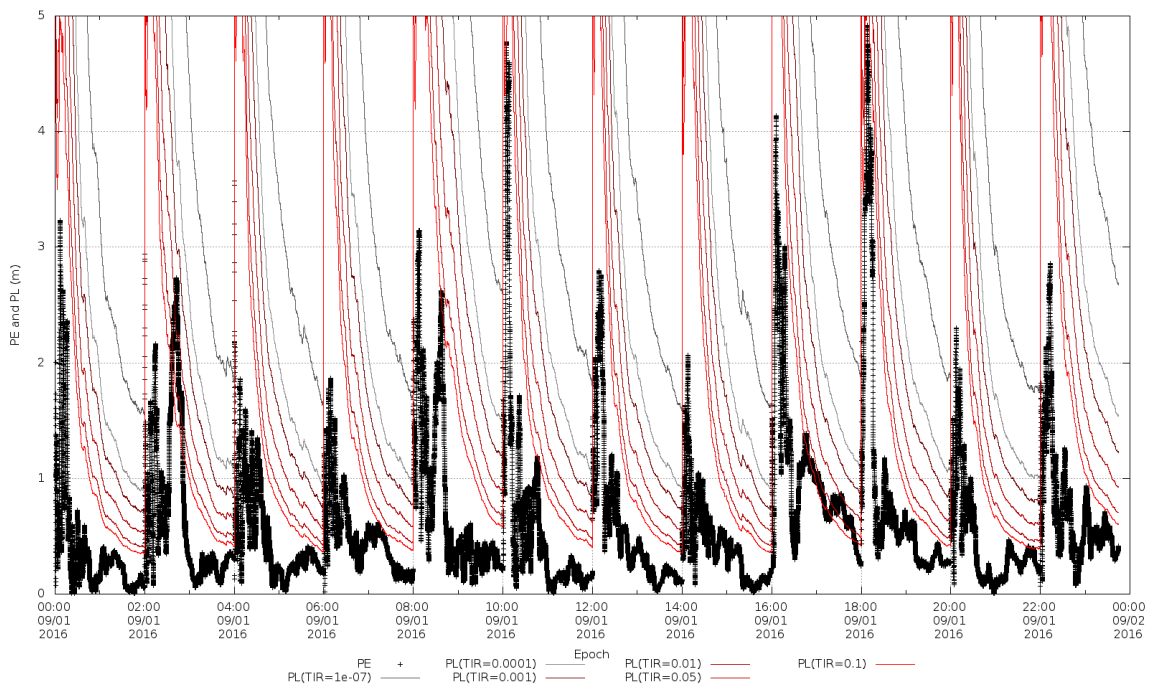


Figure 15: Position Error and PL – Horizontal

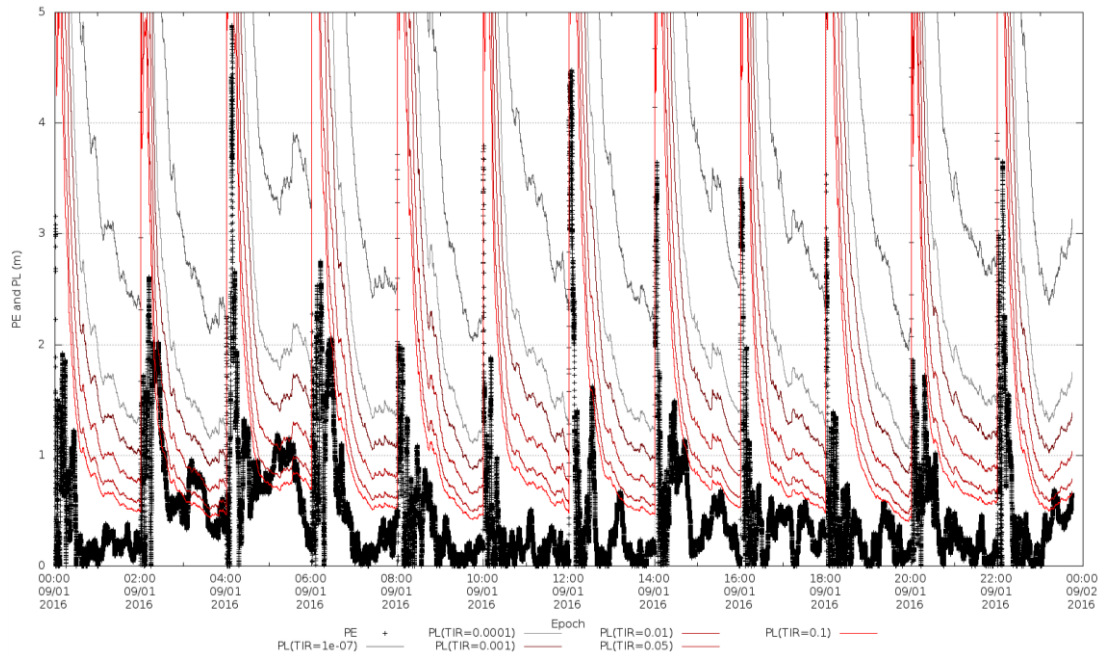


Figure 16: Position Error and PL - Vertical

Comparing Figure 13 and Figure 14 with Figure 15 and Figure 16, it can be seen that the range of the position error is different when using a geodetic receiver than when using a low-cost one, but the behaviour of the integrity algorithm is the same. The adjustment of the protection level values to the different type of receiver is obtained automatically by the design of the algorithm, not by changing its configuration in each case. This is one of the main strengths of the algorithm.

Test Case 4: Kinematic 1: Urban, geodetic receiver

The fourth Test Case corresponds to a kinematic urban trajectory around the train station area in Colmenar Viejo,

a town near the GMV premises, and a two symmetric stretches (go and return ways) through the Colmenar Viejo – Hoyo de Manzanares connecting towns road. Colmenar Viejo is about 30 km north from Madrid. Figure 17 below shows the trajectory driven through. It includes two special locations: the first one is a particular area with a higher density of trees, which results in the fact that GNSS signals are lost when the vehicle goes through it, and the second one is a bridge over the road. Both of them are depicted in Figure 18 below, together with a more standard building area, on the right.

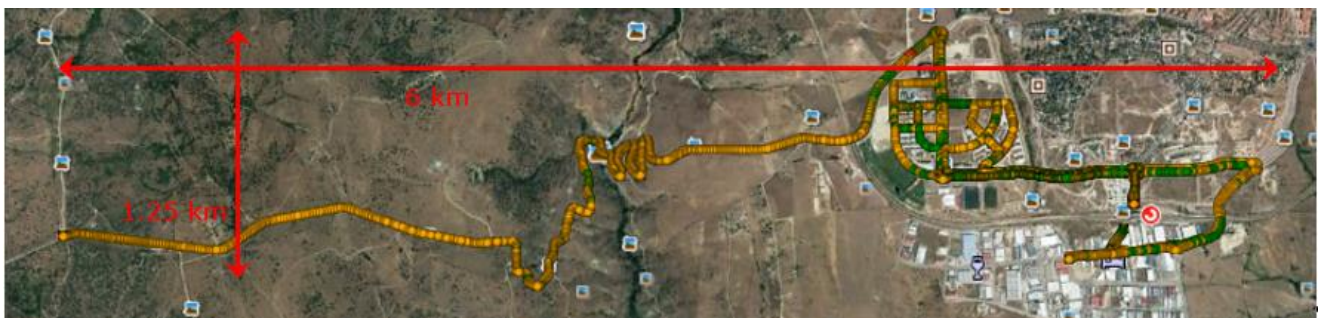


Figure 17: Kinematic trajectory



Figure 18: Different trajectory locations: Dense tree area (left), bridge over road (middle), buildings area (right)

The total scenario covers a whole period of about two hours. The pure kinematic part lasts for about 1 hour 15 minutes, whereas the first 45 minutes were reserved for the PPP process convergence. Note that 45 minutes is more than enough for the process to converge! The timeline of the test can be summarised as follows:

- Test starts: 08/05/2016, about 08:32 UTC.
- The vehicle remains stopped until 08:38.
- The vehicle is moving while converging for about 4 minutes.
- At about 08:42 the vehicle is stopped at a certain location and is kept there until 09:16 approx. The PPP position solution obtained at this location (we can call it “reference point”) before the pure kinematic trajectory is begun will be compared with other values obtained at the same location when the vehicle is returned to it several times as part of the kinematic period. The consistency between the different obtained values will be used to analyse the PPP process behaviour, as a complement to the RTK based reference trajectory.
- Kinematic trajectory begins at about 09:16.
- The vehicle is returned to the “reference point” at about 09:29.
- At about 09:32, the vehicle goes through the dense tree area depicted in Figure 18 above (left picture).
- About 09:36, the vehicle is stopped again at the “reference point”.
- At about 09:47, the vehicle goes again through the mentioned dense tree area.
- At about 09:49 the vehicle is stopped again at the “reference point”.
- At about 09:53 the vehicle goes again through the mentioned dense tree area.
- At about 09:56 the vehicle is stopped again at the “reference point”.
- At about 10:05 the vehicle goes under the bridge over the road depicted in Figure 18 above (middle picture).
- At about 10:05 the vehicle goes again under the bridge over the road depicted in Figure 18 above (right picture), in the return way.
- At about 10:27 the vehicle is stopped for the last time at the “reference point”.
- At about 10:28 the test ends.

The PPP process has been run, with the gap-bridging option activated, in parallel with the integrity algorithm configured for different integrity risk levels, and a dedicated RTK process carried out with the aim of using it as reference for the associated accuracy and accuracy/integrity analyses. The measurements processed correspond to the GPS and GLONASS constellations.

GAP4 has been used as base station. It is located on the roof of the GMV premises at Tres Cantos, about 10 km away from the Test Case locations, in the South-East direction. The relative position between the Test Case trajectory and the Reference (Station) Position is depicted in Figure 19 below. Please note that the obtained RTK solution is not continuous, since ambiguities have not been able to be solved for all the epochs in the considered time period. For this reason, there are some gaps in depicting the error of the PPP process when compared to the RTK solution.

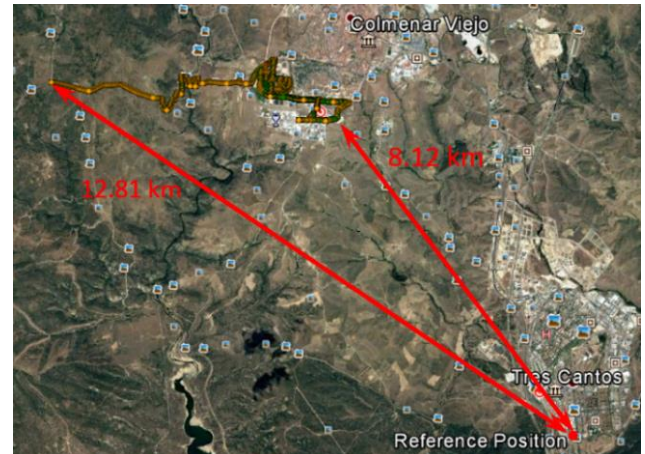


Figure 19: Test Case locations and Reference (Station) position relative positions

Autonomous consistency checks have also been carried out, comparing the different PPP position solutions obtained when stopping the vehicle at the “reference point”, before, during and at the end of the kinematic period.

The obtained results are summarised next. Table 4 below contains the experimental rate of integrity failures for six different integrity risk values, for horizontal and vertical errors, which is within the target in all cases

Table 4: Relative rate of integrity failures in Test Case 4 for different Target Integrity Risk (TIR) values

TIR	0.1	0.05	0.01	0.001	1e-04	1e-07
H	0	0	0	0	0	0
V	0.69	0.37	0.06	0.1	0	0

The following figures show the obtained results in terms of accuracy and integrity. Figure 20 shows the PPP position horizontal solution error with respect to the reference RTK trajectory, together with the obtained PLs for the different integrity risk values, and Figure 21 shows the analogous results for the vertical component.

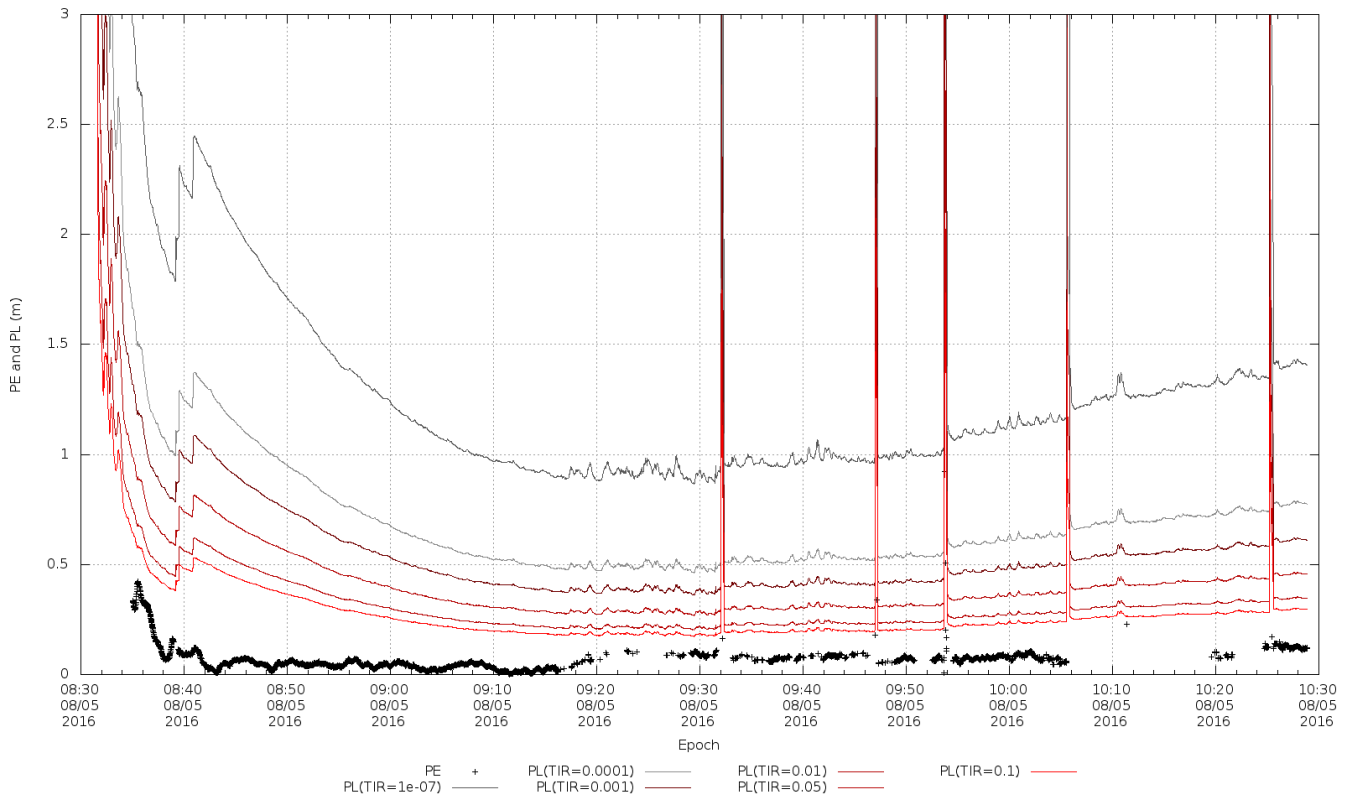


Figure 20: Position Error and PL – Horizontal

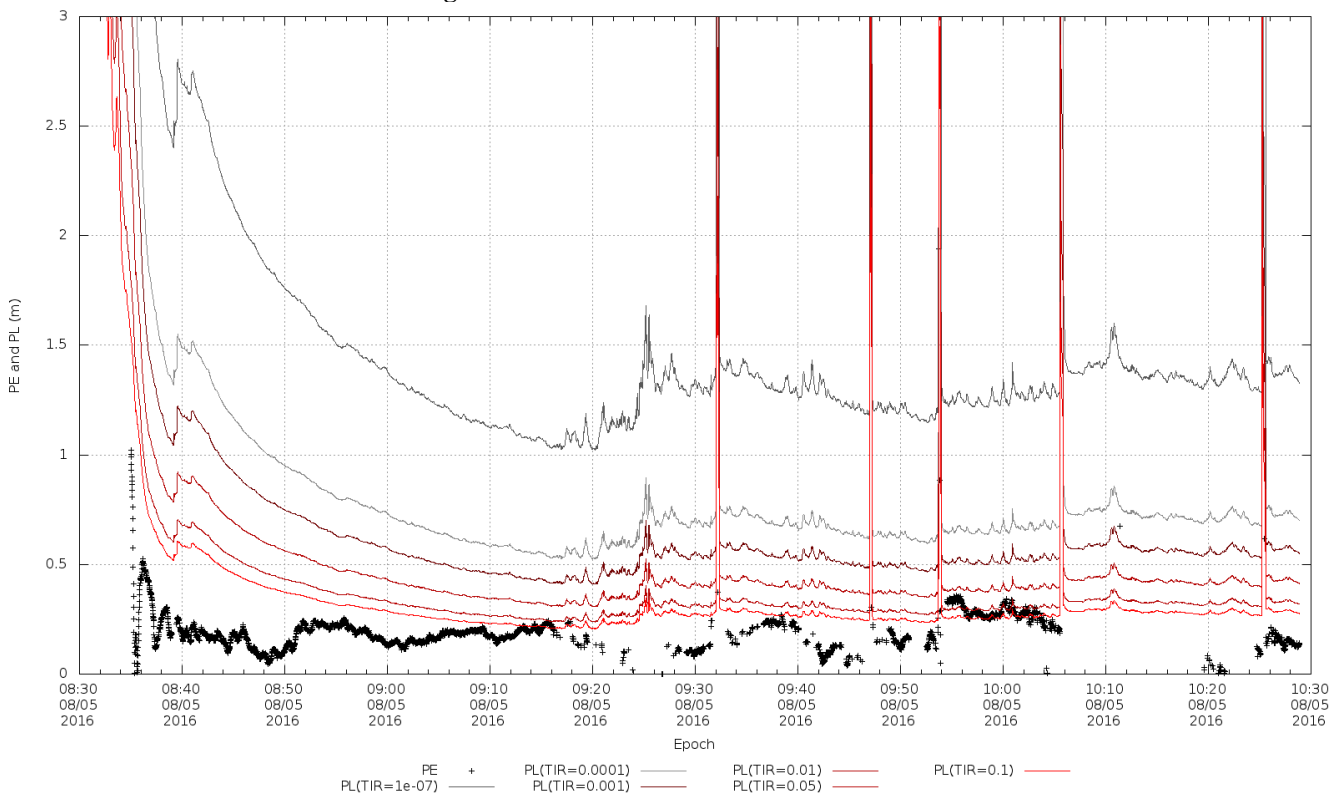


Figure 21: Position Error and PL – Vertical

It is especially interesting to pay attention to the magnitude of the obtained protection levels, which:

- Are able to follow the process convergence
- Move in a relatively low range, even for demanding TIR values
- Are able to react to the observability problems (gaps when lines of sight are lost), generating PL values out of the standard range
- Return to the typical range soon after the lost lines of sight are recovered

It is also remarkable how the gap-bridging algorithm brings continuity to the solution when the carrier-phase ambiguities are broken by obstacles. At the epochs where the carrier-phase continuity is lost, there is a brief period of some seconds, until the gap-bridging resolution is effective, where the protection levels have a peak. This is precisely the desired behaviour.

As regards the size of the protection levels, in this scenario with urban parts it is higher than in the converged open-sky conditions, but still they are not far from 1 meter for the smallest TIR considered.

Figure 22 and Figure 23 show the results of the autonomous consistency checks performed for the vertical component.

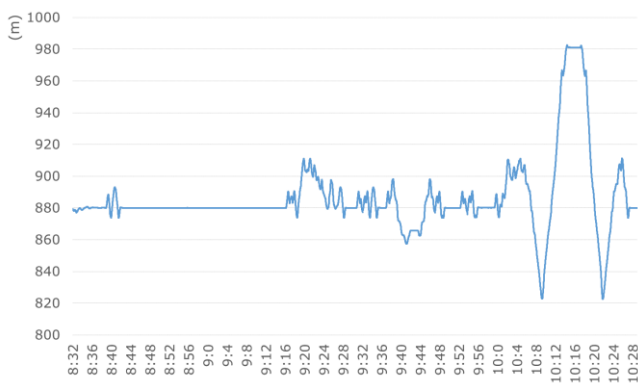


Figure 22: PPP Positioning Solution (Vertical)

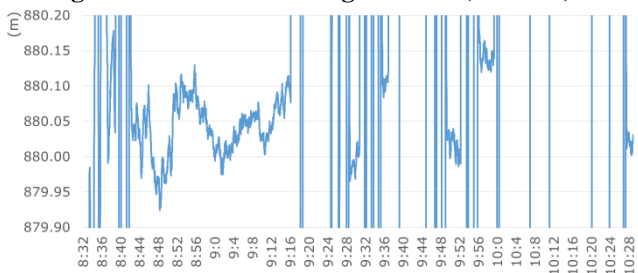


Figure 23: PPP Positioning Solution (Vertical) - Zoom

During the time the vehicle is stopped after the first convergence minutes, and at all the times the vehicle is returned to the “reference point”, the vertical solution is quite consistent. It remains in a 20-30 cm range, even if the vehicle has gone through definitely complicated locations, and has to have recovered from five all lines of sight losses.

Test Case 5: Kinematic 2: Urban, low-cost receiver

This test case consists in the same kinematic trajectory as in the previous one, but analysing the results using a low-cost receiver. Driven by the enhancement of mobile

technology, among others, in the recent years low-cost receivers have undergone a massive improvement and mass-market applications where PPP techniques are used have appeared. It is because this that it is important to improve the PPP performance when using low-cost receivers. The receiver model is U-BLOX NEO-M8N, connected to a low-cost patch antenna. It provides single-frequency measurements from GPS and GLONASS satellites.

Table 5 below contains the experimental rate of integrity failures for six different integrity risk values, for horizontal and vertical errors, which is below the target in all cases.

Table 5: Relative rate of integrity failures in Test Case 5 for different Target Integrity Risk (TIR) values

TIR	0.1	0.05	0.01	0.001	1e-04	1e-07
H	0.80	0.08	0	0	0	0
V	0.59	0.69	0	0	0	0

The following figures show the obtained results in terms of accuracy and integrity. As in the previous case when using the geodetic receiver, Figure 24 shows the PPP position horizontal solution error with respect to the reference RTK trajectory, together with the obtained PLs for the different integrity risk values, and Figure 25 shows the analogous results for the vertical component.

As in the previous case, the algorithm is able to follow the convergence period, react when observability problems occur and return to typical values after the lines of sight are recovered. The difference with respect to the case using a geodetic receiver is that the errors comparing with the RTK reference are larger when using the low-cost receiver. The comparison of the RMS of the errors for the North, East and Up components are shown in Table 6 below:

Table 6: Comparison of RMS error using a geodetic or a low-cost receiver

Receiver	RMS Error North (m)	RMS Error East (m)	RMS Error Up (m)
Geodetic	0.041	0.079	0.209
Low-Cost	0.777	0.653	1.521

In spite of that, the integrity failures obtained for six different integrity risk values, for horizontal and vertical errors, are below the target integrity. The reason is that the protection levels are higher in this case, showing the adaption capabilities of the KIPL algorithm. With all, it has been showed that the integrity algorithm gives good results no matter the receiver type, which is one of the main characteristics required in order to be able to cover all the mass-market demands.

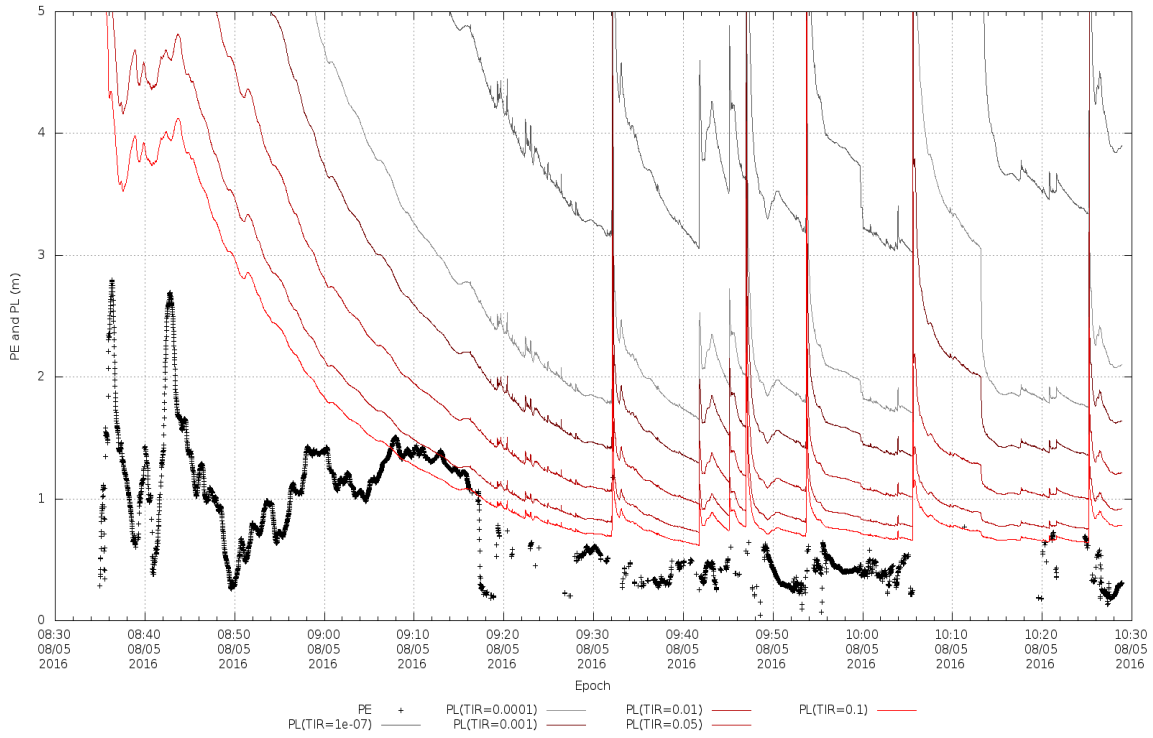


Figure 24: Position Error and PL – Horizontal

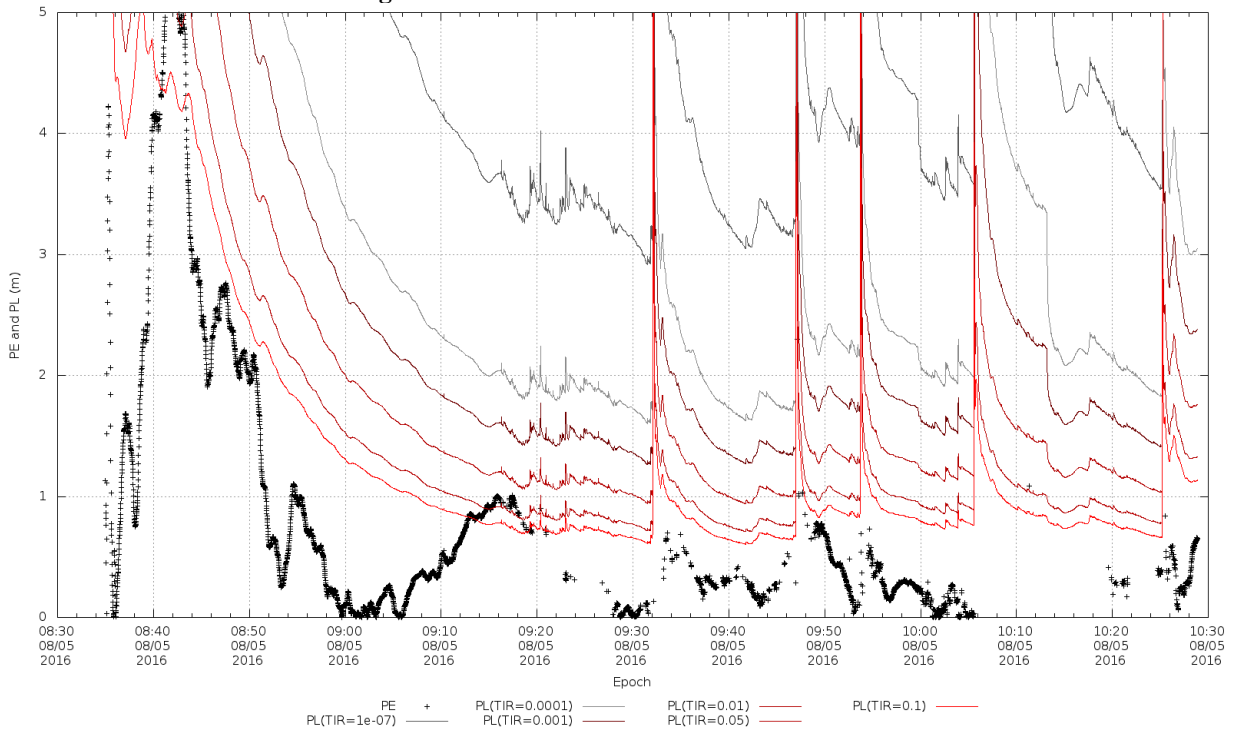


Figure 25: Position Error and PL - Vertical

Test Case 6: Kinematic 3: Urban, geodetic receiver, including Galileo

In this test, the trajectory is obtained by processing data from GPS and Galileo satellites. In particular, there are measurements from four Galileo satellites: E11, E12, E19, E24. A geodetic receiver (Trimble R10), placed on the top

of a car, has been used to record the data. The timeline of the test can be summarised as follows:

- Test starts: 08/31/2016, about 11:42 UTC.
- The vehicle remains in the same position until 12:16.
- The vehicle is moving in open-sky conditions from 12:16 to 12:57.
- From 12:57 onwards, the vehicle is moving through an urban area in Tres Cantos.

Table 7 and Table 8 below contain the experimental rate of integrity failures for six different integrity risk values, for horizontal and vertical errors, which is below the target in all cases. Two configurations are considered: GPS-only and GPS+Galileo.

Table 7: Relative rate of integrity failures in Test Case 6, GPS+Galileo, for different TIR values

TIR	0.1	0.05	0.01	0.001	1e-04	1e-07
H	0.03	0	0	0	0	0
V	0.14	0.06	0.04	0	0	0

Table 8: Relative rate of integrity failures in Test Case 6, GPS-only, for different TIR values

TIR	0.1	0.05	0.01	0.001	1e-04	1e-07
H	0.02	0.02	0.06	0	0	0
V	0.39	0.22	0.08	0	0	0

The following figures show the PPP position horizontal and vertical errors with respect to the reference RTK trajectory, together with the obtained PLs for the different integrity risk values. The results for the GPS+Galileo and GPS-only solutions are provided. The initial error is very small as we start from a calibrated position.

As in the previous scenarios, the integrity failures are always below the target integrity. The most relevant feature in this case is the behaviour of Protection Levels during the final urban phase of the trajectory. In the GPS-only configuration they take higher values and have a more irregular behaviour. The reason is that in that case there are epochs when only a few satellites are in view, and then there must be less confidence in the solution obtained. It is not only that the solution may be less accurate, but also that the power of the indicators to detect any type of degradation is smaller.

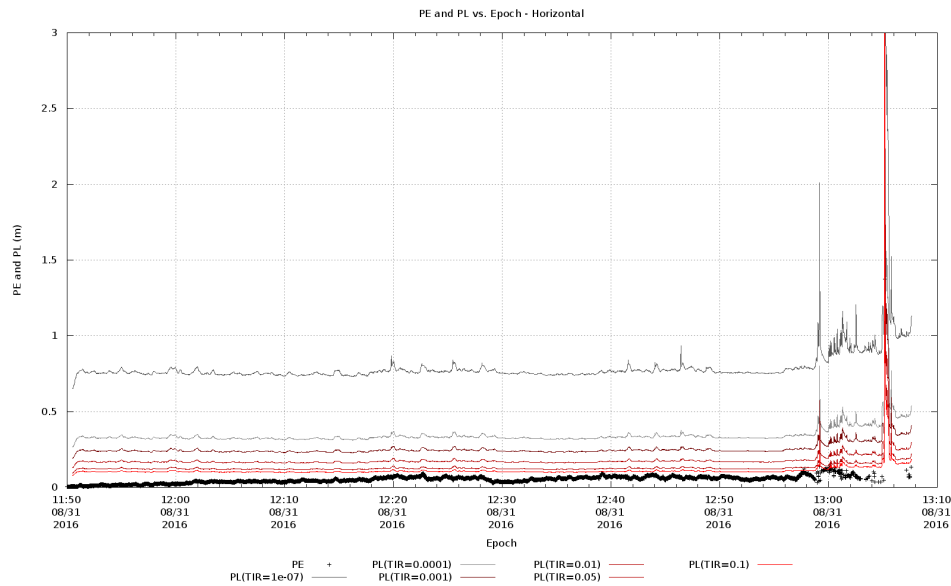


Figure 26: Position Error and PL – Horizontal – GPS+Galileo

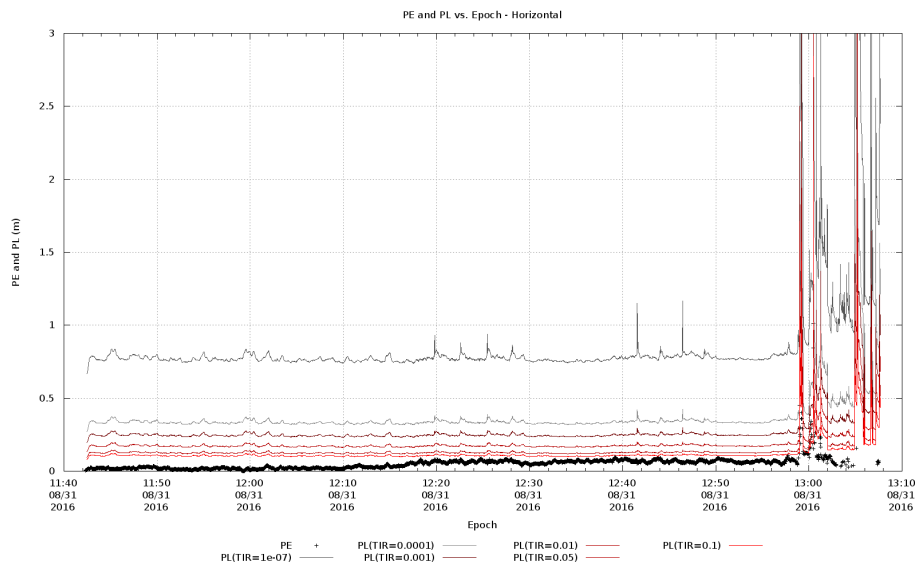


Figure 27: Position Error and PL – Horizontal – GPS-only

PRELIMINARY SAFETY ANALYSIS

As mentioned in the introductory sections, the classical approach of dividing the possible cases in a controlled nominal case with a simple characterization of the errors plus a set of faults or Feared Events that can occur with a small probability is too simplistic for many land users. For instance, if the receiver is in a car, each time it goes through an urban area there will be a number of simultaneous problems (NLOS, carrier-phase-losses, ...) that will be changing as the car moves. The first task of a realistic integrity method for road applications is to cope with such situations, which are not exceptional events, but part of the usual conditions.

The KIPL algorithm has shown very good performance in different conditions, including urban areas. As an example, Figure 28 shows a Stanford diagram obtained from an extensive campaign including urban canyons in Madrid, by using a standard Kalman filter solution based on pseudorange and Doppler measurements plus IMU data from a low-cost chip, (see [Ref. 13.] for more information). These results have been confirmed in the case of the PPP in all the scenarios processed in urban areas.

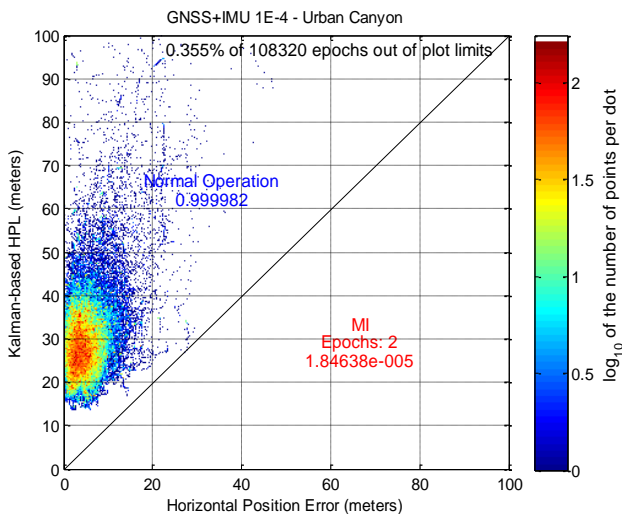


Figure 28 Stanford diagram, HPL GNSS+IMU, TIR =1E-4, Urban canyon

Nevertheless, it is important to complement the experimental validation of the algorithm with a rigorous analysis of how the KIPL algorithm behaves in the presence of faults. The analysis will indicate which enhancements of the KIPL design and/or implementation are needed to make it more powerful and it will be a first step towards a potential certification process.

Hence, in order to provide a more complete view of the PPP+KIPL behaviour, a preliminary safety analysis has been performed. It consists of a Fault Tree Analysis (FTA) and a Failure Mode Effects and Criticality Analysis (FMECA). FTA and FMECA are complementary analyses

that allow obtaining a comprehensive understanding of the system failures.

Fault trees are classic deductive (top-down) analysis technique, which works from undesired event to basic causes and it has become by far the most commonly used deductive safety analysis technique. A fault tree represents graphically the combinations of events and conditions that contribute to the occurrence of a single undesirable event, called the top event. In this case, the top event to be analyzed is a miscalculation by KIPL algorithm triggering an integrity failure.

Three types of error have been considered to contribute to a miscalculation:

- **Measurement errors:** This is expected to be the main source of errors, derived from the noise and the temporal correlation of the filtered solutions.
- **Propagation errors:** Those errors derived from the lack of accuracy when the solution is propagated to the next epoch.
- **Model errors:** Those errors derived from the imperfections of the physical models used in the reconstruction of the measurement.

The FMECA is a classic inductive (bottom-up) analysis technique, which considers each single elementary failure mode and assessing its effects up to the boundary of the product or process under analysis. Its methodology is not adapted to assess combination of failures within a product or a process. The FMECA, is an effective tool in the decision making process, provided it is a timely and iterative activity.

Some standard failures have been considered to perform this preliminary safety analysis. Magnitude considered in the analysis are supposed to be representative, though precise values for each of the considered failures could be further refined as more detailed information is obtained. Figure 29 and Figure 30 show the fault-trees that have been elaborated as part of this preliminary safety analysis.

- Figure 29 shows general FTA when considering the user is operating a geodetic receiver in an open sky environment. The undeveloped event “measurement errors” has been analyzed separately. Satellite position and clock errors have been taken into account too. The symbols represent events, conditions and logical operators (AND and OR gates).
- Figure 30 represents general FTA when considering the user is operating a low-cost receiver in a more constrained environment. As well as in previous figure, undeveloped event “measurement errors” has been analyzed separately. Satellite position and clock errors have been taken into account too. It can be traced to Test Case 5 (kinematic, low-cost receiver).

The FMECA parameters are described in Table 9 below:

Column	Description
Failure mode	Identification and brief description of the assumed failure mode at item level. Failure modes that can propagate to interfacing functions elements shall be identified
Next Higher Effect	Brief description of the failure mode consequences on the higher level function.
End effects	Effect that the assumed failure mode has on the operation, function, or status of the element and its interfaces assuming that the compensation if any (redundancy etc.) is fully operational.
Severity	Severity classification category according to the worst potential end effect of the failure. It is considered 4 severity levels (being IV the lowest and I the highest) according to the failure impact on system availability and reliability.
Failure rate	Frequency with which the failure mode takes place. It represents the average failures per hour in a continuous operation.
Compensation	Indicates the potential means (redundancy, safety device etc.) and operations (operational procedure etc.) to recover the function to acceptable degraded consequences. For the critical failure modes which cannot be eliminated, justification shall be provided showing that all reasonable action have been implemented which allow the acceptance of the design.

The FMECA analysis is presented in Table 10.

Figure 29 represents the FTA for open sky with geodetic receiver. The three mentioned sources of error (plus the reference system error) have been considered, and they represent the four branches of the tree:

1. Propagation error: They are assumed to be triggered by stochastic mismodelling of Kalman filter.
2. Reference system error: This branch is actually a single event, the Reference system error, which is an external element considered in this tree.
3. Model error: It considers that server corrections checks and PPP detection can act as barriers to product errors. Since we are considering the existence of several barriers, the contribution of this branch to the general tree is minor.
4. Measurement error. This branch considers not only the errors affected by the environment, but also those whose failure rate is higher when using a low-cost receiver.

Figure 30 is the FTA for low cost receiver and unfavorable (urban) environment. The structure of the analysis is analogous to that of the FTA for the open sky-geodetic receiver environment. Propagation error, reference system error and model error are the same in both cases. Yellow boxes represent barriers to errors, and green event are external events. The “measurement error” has been analysed separately. Note that the contribution of this branch is higher in the constrained urban low-cost environment, consequently increasing the global failure rate, which is 0.000606 failures/hour, in the open sky-geodetic case, and 0.00587 failures/hour in the more constrained (urban) – low-cost case.

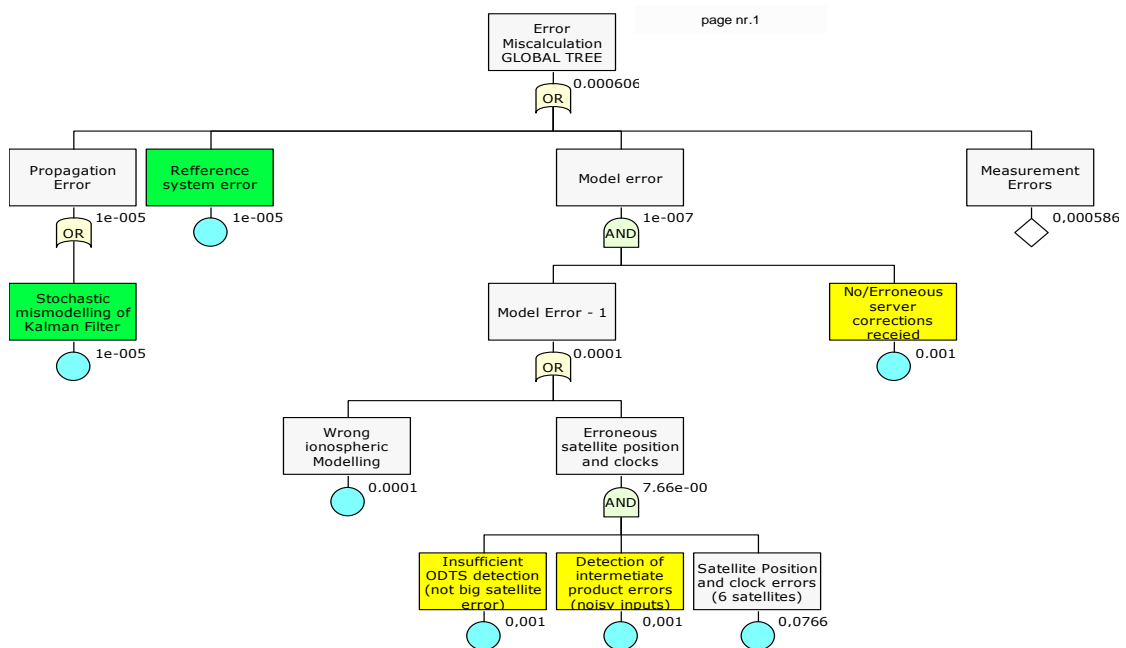


Figure 29: Global FTAs open sky-geodetic

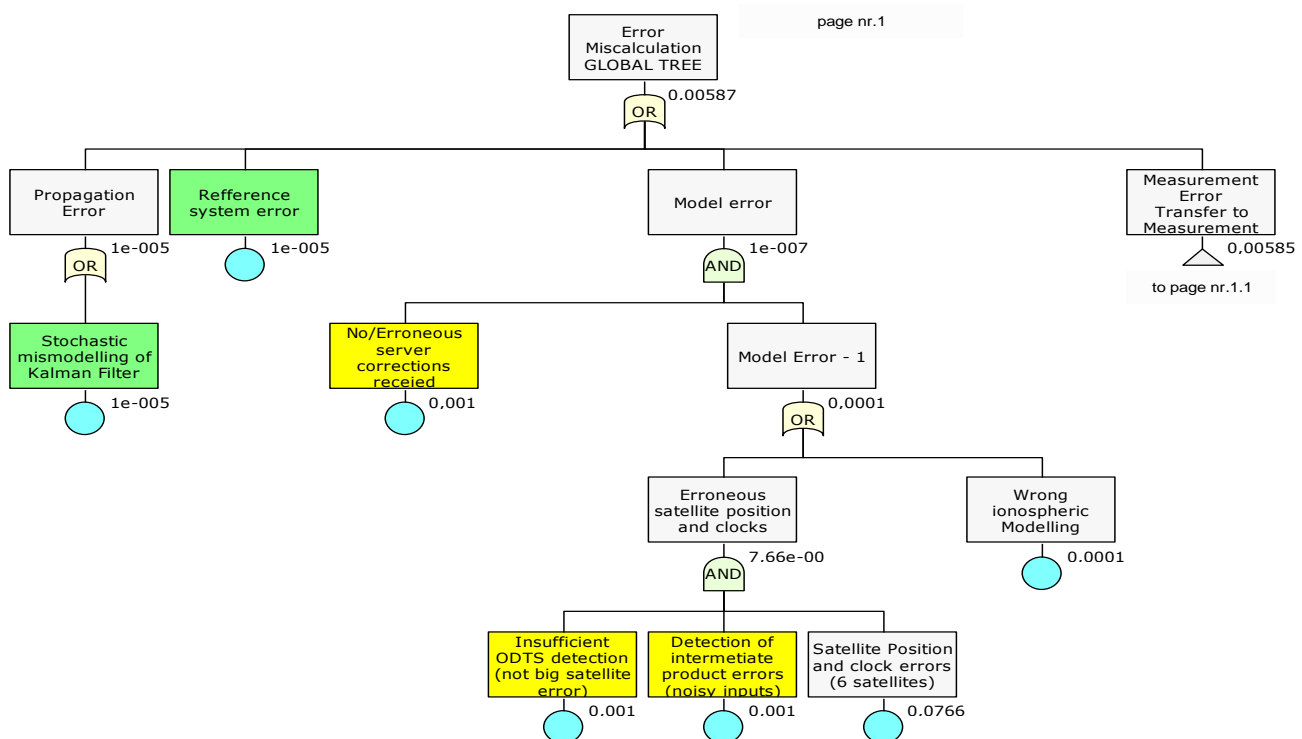


Figure 30: Global FTA constrained urban-low-cost

To analyze measurement errors, the following events have been taken into account:

1. Cycle slips: discontinuities in the phase measurements that are seen as jumps of integer number of wavelength.
2. Oversize errors. The algorithm could be unable to properly manage excessively large errors.
3. Errors correlation: It is important to include the effect of correlations. High correlation values can result in the filter to produce solutions with bigger errors. The main variable is a correlation matrix, which is updated at each epoch. Some hazards like a ramp or offset biases can increase the probability of an insufficient correlation estimation.

Some barriers, such as correlation estimation and multipath detection filter have been considered. In particular, correlation estimation barrier avoids errors due to receiver problems, such as ramp or offset biases and other undesirable effects. In this preliminary analysis, approximate values have been used for some of the contributions, like the oversize errors failure rate. The magnitudes can be assumed to be right, whereas the exact values can be subject to further refinement.

This analysis has been performed too for favourable and unfavourable conditions. For most of the hazards, the failure rates are significantly higher in urban environment

than in open sky. The main factor limiting performance is the reduced observability due to the environment, hence the larger magnitude order for the measurement error failure rate.

Failure rate obtained for measurement errors is 0.000586 with favorable conditions and 0.00585 with unfavorable conditions.

Our analysis of satellite position and clock errors (which is not shown in this paper) include all GPS and GALILEO external feared events to be taken into account for PPP algorithm. Failure rates are standard data from space projects. For those cases where GPS and GALIEO values were different, a conservative approximation has been followed and the worst number has been included in the analysis. Failure rate obtained for satellite position and clock error is 0.00132.

The following table presents FMECA, which is a bottom-up analysis that consists of the identification of system failure modes, analyzing their local effects, barriers and revealing single points of failure. In our case, identified barriers are the following ones: correlation estimation, PPP detection and multipath detection filter, which can prevent most of failure modes to have an undesired effect.

The FMECA table is detailed hereunder:

Table 10: FMECA Analysis

Failure Mode	Next Higher effect	End Effect	Severity	Failure Rate	Compensating Provisions
Bias that remains in time	No effect (correlation estimation barrier implemented)	No effect	IV	0.001	Correlation estimation
Code Carrier Incoherency	Satellite position and clock error	No effect (PPP detection)	IV	1e-005	PPP detection
Cycle slip errors	Measurement error	Error Miscalculation	I	0.0036	
Degraded EIRP	Satellite position and clock error	No effect (PPP detection)	IV	0.0001	PPP detection
Degraded carrier phase	Satellite position and clock error	No effect (PPP detection)	IV	2.5e-006	PPP detection
Detection of intermediate product errors (noisy inputs)	No effect	No effect	IV	0.001	
Erroneous Broadcast clock	Satellite position and clock error	No effect (PPP detection)	IV	0.0001	PPP detection
Erroneous Navigation Message	Satellite position and clock error	No effect (PPP detection)	IV	0.0001	PPP detection
Erroneous broadcast orbits	Satellite position and clock error	No effect (PPP detection)	IV	0.0001	PPP detection
Evil Wave Form	Satellite position and clock error	No effect (PPP detection)	IV	0.0001	PPP detection
Filter does not detect multipath	No effect	No effect	IV	0.001	
Insufficient PPP detection (not big satellite error)	No effect	No effect	IV	0.001	
Insufficient correlation estimation	No effect	No effect	IV	0.001	
Issue of data anomaly	Satellite position and clock error	No effect (PPP detection)	IV	1e-006	PPP detection
Loss of SV Signal	Satellite position and clock error	No effect (PPP detection)	IV	0.0005	PPP detection
Multipath (erroneous and good signal are received)-1	No effect (multipath detection filter implemented)	No effect	IV	0.01	Multipath detection filter
Multiple Failures	Satellite position and clock error	No effect (PPP detection)	IV	5e-007	PPP detection
No/Erroneous server corrections received	No effect	No effect	IV	0.001	
Only wrong signal is detected	Measurement error	Error Miscalculation	I	0.00125	
Oversize errors	Measurement error	Error Miscalculation	I	0.001	
Pseudorange acceleration error	Satellite position and clock error	No effect (PPP detection)	IV	0.0001	PPP detection
Pseudorange drift error	Satellite position and clock error	No effect (PPP detection)	IV	0.001	PPP detection
Pseudorange step error	Satellite position and clock error	No effect (PPP detection)	IV	0.0001	PPP detection
Ramp bias	No effect (Correlation estimation barrier implemented)	No effect	IV	0.001	Correlation estimation
Reference system error	Error miscalculation	Error Miscalculation	I	1e-005	
SV Hardware Bias Drift	Satellite position and clock error	No effect (PPP detection)	IV	5e-006	PPP detection
SV Hardware Bias Jump	Satellite position and clock error	No effect (PPP detection)	IV	5e-006	PPP detection
Satellite Position and clock errors (6 satellites)	Model error	Error Miscalculation	I	0.0766	
Stochastic mismodeling of Kalman Filter	Propagation error	Error Miscalculation	I	1e-005	
Wrong ionospheric Modelling	Model error	Error Miscalculation	I	0.0001	

In this analysis, both barriers and external events have been taken into account. Most of the failure modes with not negligible consequences have already a barrier acting as a compensating provision. For this preliminary analysis, failure rates considered for most failure modes should be refined in further versions. For instance, it would be desirable to have a contribution describing the quality of products from a server.

In light of the FTA and FMECA performed analyses, some preliminary conclusions can already be drawn.

As it was expected, the main contributors are measurement errors, which represent 90% of total failure rate. However, the weight of this contributions varies substantially between the two considered scenarios: failure rates are 0.00585 failures per hour for low cost receiver and urban environment and 0.000586 for open sky and geodetic receiver. Note that the difference is about one magnitude order large. For this reason, failure rate for the worst case tree is almost ten times higher than the general tree (0.00587 failures per hours and 0.000606 failures per hour, respectively). However, it has to be highlighted that, for most urban navigation applications (e.g. automatic driving), PPP will probably be used not alone, but in combination with other non-GNSS technologies, which would act as external “barriers” if considered in a further safety analysis.

Global failure rate has also been analysed has also been analysed excluding the “Server corrections received” barrier, which is indeed pending on implementation. The performed analyses show that failure rates increase beyond 20% in case of open sky (from 0.000586 to 0.000706) and about 2% in case of urban environment (from 0.00585 to 0.00597), when the mentioned barrier is not activated. Thus, it is strongly recommended to implement it in order to significantly reduce failure rates. Note that in previous PPP integrity analyses off-line post-processed products were used instead of real time products, and the impact of the “Server corrections received” barrier on the obtained results would have been much smaller.

Additionally, in order to reduce the failure rate to even lower values, a lower bound for protection levels (PL) could be implemented in the algorithm. This lower bound would be low enough to avoid affecting the availability of the system but would avoid the loss of integrity in some cases, especially in open sky applications, where PLs are significantly lower. This lower bound would be especially helpful at epochs at which the error was very low, and the associated PL was still lower. In those cases, not having a lower bound for the PL would result in an integrity failure, which could be easily avoided without compromising the system availability.

For further versions of this preliminary safety analysis, it would be desirable have more accurate failure rates data. In addition to this, a deeper analysis should be performed

taking account data from future test cases. These are living analysis that will be updated during the course of the system life cycle, and will interact with the algorithm design identifying updates to make it more reliable.

FURTHER WORK

We are going to keep on working continuously improving the capabilities and performances of the considered KIPL PPP bounding computation. We will keep on putting it at test, in increasingly challenging conditions, with the aim of consolidating it as a reference PPP integrity/reliability algorithm, properly balanced half way between the system and the user integrity solutions, enriching the current offer of integrity for navigation solutions.

In particular, we have identified the following four specific improvement areas:

- PPP positioning bounding in enhanced supported convergences
- Design & implementation of the “Server corrections received” barrier
- PPP positioning bounding in highly demanding environments, in combination with other non-GNSS technologies
- Detection and response to feared events

Regional corrections can be computed at server level and transmitted through a regional network, for improving the convergence time. It would be really interesting to analyse the behaviour of the PPP integrity algorithm when the mentioned corrections are being used for improving the PPP process convergence.

Additionally, the PPP integrity algorithm should be upgraded for being able to manage certain information about the orbit and clock products quality, assumed to have been generated at server level, able to feed a “Server corrections received” barrier, aimed at triggering integrity failures associated to problems in the products generation.

The moderate performances of GNSS are preventing it from being used to a large extent for extremely demanding applications. PPP complemented with the additional integrity layer provided by the KIPL algorithm, could be used alone or in combination with other non-GNSS technologies for fulfilling the most demanding accuracy/integrity requirements, such as autonomous driving, precision agriculture, LBS, etc.

Some hazards like a ramp or offset biases in the measurements can increase the probability of an insufficient correlation estimation, increasing the probability of integrity failures. These and other feared events will be carefully identified and analysed, in order to implement proper detection and mitigation dedicated strategies.

With regard to the continuous enhancement of the PPP integrity computation capabilities and performances, the main activities include:

- Extensive experimentation, enriched with the generated feedback of the previous results, trying to cope with and increasing wide range of difficulties in all kind of environments
- Sustained OD&TS process improvement, ensuring excellent orbit and clock products performances
- Sustained PPP process improvement, enhancing robustness and accuracy of the provided solutions

CONCLUSIONS

- PPP is consolidated as an alternative/complement to RTK for high accuracy positioning applications
- The PPP integrity bounds provided by the KIPL algorithm are in the centimetric/decimetric range, providing integrity failures percentages in the required intervals for different integrity TIR values in the different analysed scenarios
- The KIPL algorithm can be considered an excellent balanced candidate half way between the system and the user integrity solutions, enriching the current offer of integrity for navigation solutions

ACKNOWLEDGEMENTS

Thank you very much to Guillermo Tobías, David Calle, Enrique Carbonell and Jorge Bullido for your inestimable support in the paper preparation. Thanks also to Miguel Azaola, Joaquín Cosmen and Carlos Moriana for all your previous work on IBPL.

REFERENCES

[Ref. 1.] "Method for Autonomous Determination of Protection Levels for GNSS Positioning Based on Navigation Residuals and an Isotropic Confidence Ratio" Patent: Europe: EP2113786 (B1), USA: US8203482 (B2).

[Ref. 2.] "Method for Autonomous Determination of Protection Levels for GNSS Positioning Based on Navigation Residuals and an Isotropic Confidence Ratio" Patent: Europe: EP2113786 (B1), USA: US8203482 (B2).

[Ref. 3.] GSA GNSS Market Report, Issue 4, March 2015, <https://www.gsa.europa.eu/market/market-report>.

[Ref. 4.] Píriz, R., Mozo, A., Navarro, P., Rodríguez, D., "magicGNSS: Precise GNSS Products Out of the Box," *Proceedings of the 21st International Technical Meeting of the Satellite Division of The Institute of Navigation (ION GNSS 2008)*, Savannah, GA, September 2008, pp. 1242-1251.

[Ref. 5.] Tobías, Guillermo, Calle, J. David, Navarro, Pedro, Rodríguez, Irma, Rodríguez, Daniel, "magicGNSS' Real-Time POD and PPP Multi-GNSS Service," *Proceedings of the 27th International Technical Meeting*

of The Satellite Division of the Institute of Navigation (ION GNSS+ 2014), Tampa, Florida, September 2014, pp. 1046-1055.

[Ref. 6.] Píriz, R., Calle, D., Mozo, A., Navarro, P., Rodríguez, D., Tobías, G., "Orbits and Clocks for GLONASS Precise-Point-Positioning," *Proceedings of the 22nd International Technical Meeting of The Satellite Division of the Institute of Navigation (ION GNSS 2009)*, Savannah, GA, September 2009, pp. 2415-2424.

[Ref. 7.] Tobias, G., Garcia, C., Mozo, A., Navarro, P., Píriz, R., Rodríguez, I., Rodríguez, D., "Filling in the gaps of RTK with Regional PPP," *Proceedings of the 24th International Technical Meeting of The Satellite Division of the Institute of Navigation (ION GNSS 2011)*, Portland, OR, September 2011, pp. 2193-2201.

[Ref. 8.] Mozo, Álvaro, Calle, J. David, Navarro, Pedro, Píriz, Ricardo, Rodríguez, Daniel, Tobías, Guillermo, "Demonstrating In-The-Field Real-Time Precise Positioning," *Proceedings of the 25th International Technical Meeting of The Satellite Division of the Institute of Navigation (ION GNSS 2012)*, Nashville, TN, September 2012, pp. 3066-3076.

[Ref. 9.] Tobías, Guillermo, Calle, J. David, Navarro, Pedro, Rodríguez, Irma, Rodríguez, Daniel, "Real-Time PPP with Galileo, Paving the Way to European High Accuracy Positioning," *Proceedings of the 27th International Technical Meeting of The Satellite Division of the Institute of Navigation (ION GNSS+ 2014)*, Tampa, Florida, September 2014, pp. 2354-2362.

[Ref. 10.] Merino, Miguel M. Romay, Lainez, Maria D., "Integrity for Advanced Precise Positioning Applications," *Proceedings of the 25th International Technical Meeting of The Satellite Division of the Institute of Navigation (ION GNSS 2012)*, Nashville, TN, September 2012, pp. 2742-2758.

[Ref. 11.] Samper, M. D. Laínez, Romay Merino, M. M., "In-The-Field Trials for Real-Time Precise Positioning and Integrity in Advanced Applications," *Proceedings of the ION 2013 Pacific PNT Meeting*, Honolulu, Hawaii, April 2013, pp. 146-167.

[Ref. 12.] Laínez Samper, María D., Romay Merino, Miguel M., Tobías González, Guillermo, Barba Martí, David, "PPP for Advanced Precise Positioning Applications, Including Reliability Bound," *Proceedings of the 27th International Technical Meeting of The Satellite Division of the Institute of Navigation (ION GNSS+ 2014)*, Tampa, Florida, September 2014, pp. 2478-2493.

[Ref. 13.] Madrid, Pedro F. Navarro, Saenz, Miguel Azaola, Varo, Carlos Moriana, Schortmann, Joaquín Cosmen, "Computing Meaningful Integrity Bounds of a Low-cost Kalman-filtered Navigation Solution in Urban Environments," *Proceedings of the 28th International*

Technical Meeting of The Satellite Division of the Institute of Navigation (ION GNSS+ 2015), Tampa, Florida, September 2015, pp. 2914-2925.

[Ref. 14.] Madrid, Pedro F. Navarro, Samper, Maria D. Laínez, Merino, Miguel M. Romay, "New Approach for Integrity Bounds Computation Applied to Advanced Precise Positioning Applications," Proceedings of the 28th International Technical Meeting of The Satellite Division of the Institute of Navigation (ION GNSS+ 2015), Tampa, Florida, September 2015, pp. 2821-2834.

[Ref. 15.] Irma Rodríguez Pérez, Guillermo Tobías González, Jesús David Calle Calle, Miguel Romay, María Dolores Laínez, Pedro F. Navarro, "Galileo, an Ace up in the Sleeve for PPP Techniques", Proceedings of the 29th International Technical Meeting of The Satellite Division of the Institute of Navigation (ION GNSS+ 2016), Portland, Oregon, September 2016.

[Ref. 16.] Cosmen-Schortmann, J.; Azaola-Saenz, M.; Martinez-Olague, M.A.; Toledo-Lopez, M.; , "Integrity in urban and road environments and its use in liability critical applications," Position, Location and Navigation Symposium, 2008 IEEE/ION , vol., no., pp.972-983, 5-8 May 2008, DOI: 10.1109/PLANS.2008.4570071

[Ref. 17.] Isotropy-Based Protection Levels: a Novel Method for Autonomous Protection Level Computation with Minimum Assumptions, Azaola Sáenz, M.; Cosmen Schortmann, J.; Martínez Olagüe, M.A.; Toledo López, M., GMV Aerospace and Defence S.A. (Spain), NAVITEC 2008, Noordwijk (The Netherlands), Dec 2008.

[Ref. 18.] Azaola Sáenz, M., Cosmen Schortmann, J. "Autonomous Integrity, An Error Isotropy-Based Approach for Multiple Fault Conditions, Inside GNSS, <http://www.insidegnss.com/auto/janfeb09-azaoli.pdf> January/February 2009, pp.28-36.

[Ref. 19.] Azaola, M., Calle, D., Mozo, A., Piriz, R., "Autonomous Isotropy-Based Integrity Using GPS and GLONASS, "Proceedings of the 23rd International Technical Meeting of The Satellite Division of the Institute of Navigation (ION GNSS 2010), Portland, OR, September 2010, pp. 2135-2147.

[Ref. 20.] Azaola, M., Moriana, C., Navarro, P., Valdés, D., Bonardi, L., Toledo, M., Cosmen, J., "Experimental Evaluation for Road User Charging of GPS/GLONASS/MEMS OBU, "Proceedings of the 26th International Technical Meeting of The Satellite Division of the Institute of Navigation (ION GNSS+ 2013), Nashville, TN, September 2013, pp. 656-666.

[Ref. 21.] Cezón, A., Cueto, M., Fernández, I., "Analysis of Multi-GNSS Service Performance Assessment: ARAIM vs. IBPL Performances Comparison, "Proceedings of the 26th International Technical Meeting of The Satellite

Division of the Institute of Navigation (ION GNSS+ 2013), Nashville, TN, September 2013, pp. 2654-2663.

[Ref. 22.] . Madrid, Pedro F. Navarro, Saenz, Miguel Azaola, Varo, Carlos Moriana, Schortmann, Joaquin Cosmen, "Computing Meaningful Integrity Bounds of a Low-cost Kalman-filtered Navigation Solution in Urban Environments," Proceedings of the 28th International Technical Meeting of The Satellite Division of the Institute of Navigation (ION GNSS+ 2015), Tampa, Florida, September 2015, pp. 2914-2925.

[Ref. 23.] ESA Navipedia, European Space Agency. navipedia.net

[Ref. 24.] http://www.gmv.com/en/space/Satellite_navigation_systems/GNSS_tools_development.html

[Ref. 25.] RTKLib by Tomoji Takasu (gpspp.sakura.ne.jp/rtklib/rtklib.htm).

[Ref. 26.] IERS Earth Orientation Data <http://www.iers.org/IERS/EN/DataProducts/EarthOrientationData/eop.html>

[Ref. 27.] IERS Conventions 2010, <http://www.iers.org/IERS/EN/Publications/TechnicalNotes/tn36.html>

[Ref. 28.] magicPPP Correction Service: http://magicgnss.gmv.com/magicGNSS_Correction_Service_Technical_Specifications.pdf